

# Gain-compensated cavities for the dynamic control of light–matter interactions

Christos Tserkezis,<sup>1,2</sup> Christian Wolff,<sup>1,2</sup> Fedor A. Shuklin,<sup>1,2</sup> Francesco Todisco,<sup>3,1,2</sup>  
Mikkel H. Eriksen,<sup>1,2</sup> P. A. D. Gonçalves,<sup>2,\*</sup> and N. Asger Mortensen<sup>1,2,4</sup>

<sup>1</sup>*POLIMA—Center for Polariton-driven Light–Matter Interactions,  
University of Southern Denmark, Campusvej 55, DK-5230 Odense M, Denmark*

<sup>2</sup>*Center for Nano Optics, University of Southern Denmark, Campusvej 55, DK-5230 Odense M, Denmark*

<sup>3</sup>*CNR NANOTEC, Institute of Nanotechnology, Via Monteroni, 73100 Lecce, Italy*

<sup>4</sup>*Danish Institute for Advanced Study, University of Southern Denmark, Campusvej 55, DK-5230 Odense M, Denmark*

(Dated: April 24, 2023)

We propose an efficient approach for actively controlling the Rabi oscillations in nanophotonic emitter–cavity analogues based on the presence of an element with optical gain. Inspired by recent developments in parity-time ( $\mathcal{PT}$ )-symmetry photonics, we show that nano- or microcavities where intrinsic losses are partially or fully compensated by an externally controllable amount of gain offer unique capabilities for manipulating the dynamics of extended (collective) excitonic emitter systems. In particular, we discuss how one can drastically modify the dynamics of the system, increase the overall occupation numbers, enhance the longevity of the Rabi oscillations, and even decelerate them to the point where their experimental observation becomes less challenging. Furthermore, we show that there is a specific gain value that leads to an exceptional point, where both emitter and cavity occupation oscillate practically in phase, with occupation numbers that can significantly exceed unity. By revisiting a recently-introduced Rabi-visibility measure, we provide robust guidelines for quantifying the coupling strength and achieving strong-coupling with adaptable Rabi frequency via loss compensation.

## I. INTRODUCTION

The possibility to control the emission of light from natural or artificial light sources at the nanoscale has been attracting considerable interest [1–7], ever since Purcell showed that the dynamics of an emitter is strongly affected by its environment [8]. The tremendous opportunities that such a control enables have kept inspiring novel designs for efficient cavities, appropriately tailored depending on the emitters under consideration. Mirror cavities, the prototypical templates in cavity quantum electrodynamics [9, 10], have long been employed as the most straightforward choice when considering atoms [11], while Bragg reflectors and photonic crystals constitute a natural option for artificial emitters such as quantum wells or dots [12, 13]. More recently, excitons in molecular aggregates or transition-metal dichalcogenides (TMDs) [14] have been introduced as emitters with strong, collective (i.e., *effective*) dipole moments, leading to the emergence, among others, of plasmonic [15–20] and Mie-resonant [21–24] nanostructures as suitable effective cavities. What really determines the appropriateness of the cavity in all these endeavours is the linewidth of the emitter: the optical mode must be chosen to have a comparable linewidth, and the coupling strength must exceed the damping rates of the individual components [1]. Nevertheless, in addition to this fundamental requirement, whatever other optical properties might characterise the cavity can readily open new routes for the manipulation of the strong-coupling response [25–28].

A major boost in the quest for photonic templates with novel, possibly “exotic” optical properties was recently provided by the adoption of the concept of non-

Hermiticity [29]. While initially introduced in the context of nuclear physics, non-Hermitian Hamiltonians eventually found a fertile playground in photonics [30], especially after the realisation that they can still have real eigenvalues, as long as they commute with the parity-time ( $\mathcal{PT}$ ) operator [31]. Their appeal in photonics is due to the fact that  $\mathcal{PT}$ -symmetric potentials can be achieved by incorporating a gain element—widely available in optics since the development of lasers—that compensates the intrinsic loss of the system [32, 33]. Explorations of  $\mathcal{PT}$  symmetry have often revealed surprising responses and intriguing novel designs, including unidirectional propagation [34–37] and cloaking [38, 39], lasers [40–42], gyroscopes [43], nanoantennas [44], and potentially powerful sensors operating at the exceptional point (EP) [45–49], i.e., the condition under which the eigenstates of the Hamiltonian coalesce and the corresponding eigenvalues are equal.

Inspired by these developments and the richness of optical phenomena that can benefit from loss–gain combinations, we explore here the possibility of designing optical cavities where the emergence and time evolution of strong coupling can be dynamically controlled through the externally provided gain. We theoretically show that by increasing the amount of gain it is possible to drive the exciton–cavity system so as to increase the number of Rabi oscillations that can be measured before damping prevails and the system completely loses its coherence. We revisit a recently-introduced visibility measure [22], and provide a detailed gain–coupling map that quantifies the different coupling regimes; based on this, one can manipulate the dynamics of the system, and accelerate or decelerate the Rabi oscillations so as to render their period more easily resolvable in experiments. Backtrack-

ing the visibility map, one can then extrapolate to infer about the properties of the coupled system in the absence of gain. Finally, we show that by further increasing the gain along specific paths, one can reach an EP, where the dynamics of the system is completely altered, and the occupations of both emitter-cavity polariton modes significantly exceed unity and oscillate nearly in-phase. This set of different behaviours indicates that inclusion of gain can open new ways for tailoring the dynamics of coupled emitter-cavity architectures, with both fundamental understanding and practical applications in mind. Analogous phenomena have already been observed for optical [50] and magnonic [51] waveguides operating at the EP, but here we generalise the treatment for any kind of collective polaritonic system. We anticipate that related experiments can readily benefit from the techniques developed in the context of  $\mathcal{PT}$  symmetry [30].

## II. HAMILTONIAN DESCRIPTION

We focus on extended, collective excitonic states like those encountered in  $J$ -aggregates, individual organic molecules, or TMDs, coupled to a (possibly open) micro- or nano-cavity such as a distributed Bragg reflector, a metallic nanoparticle, or simply a pair of mirrors, as suggested by the schematic of Fig. 1. Expressing all the interactions in terms of the actual Hamiltonian of the system becomes thus cumbersome, since one should include interaction among excitons [52], together with the appropriate Lindblad operators to account for both loss and gain [53]. We therefore restrict ourselves to a toy-model description that essentially follows classical coupled-mode theory [54]. We thus formulate the coupling problem in terms of a (semiclassical) interaction Hamiltonian. To make the description as widely applicable as possible, we consider a generic excitonic material, modelled by a simple Lorentzian permittivity, with transition frequency  $\omega_x$  and intrinsic linewidth  $\gamma_x$ , coupled to a cavity with resonance frequency  $\omega_c$  and damping rate  $\gamma_c$ . Within this description, the dynamics is then governed by the Schrödinger-like equation

$$\begin{pmatrix} \omega_c - i\frac{\gamma_c}{2} + i\frac{\gamma_g}{2} & g \\ g & \omega_x - i\frac{\gamma_x}{2} \end{pmatrix} \begin{pmatrix} a(t) \\ b(t) \end{pmatrix} = i\frac{\partial}{\partial t} \begin{pmatrix} a(t) \\ b(t) \end{pmatrix}, \quad (1)$$

where  $g$  is the coupling constant and  $\gamma_g$  is a possible gain rate added to the cavity. What we aim to explore here is if, and to what extent, the latter can be used as a means for loss compensation that would eventually enhance the visibility of Rabi-like oscillations in the strong-coupling regime. A schematic of a typical cavity composed of two mirrors is shown in Fig. 1. A quantum emitter (QE), sketched in the figure as a generic bosonic [55] system that could correspond to the TMD shown in the zoom-in, characterised by an “overall, effective emitter” dipole

moment, is placed between the two resonators, and couples to a single cavity-mode when the detuning  $\omega_x - \omega_c$  is sufficiently small. In addition to the usual characteristics of such cavities, as encountered in quantum optics, a gain element is also included here (Fig. 1), e.g., by the inclusion of an active material that does not interact with the QE, or via asymmetric pumping [56]. While, for our purposes, it is sufficient to accept that some gain mechanism can exist, it should be acknowledged that precise control of the gain rate is in practice a challenging task, which requires carefully designed experiments, appropriately adapted to the gain medium of choice—which, ideally, should have a linewidth comparable to those of the emitter and the cavity. Possibilities include electrochemical doping for quantum dots [57] or TMDs [58], spatial modulation [59], state-resolved optical pumping [60] and host-guest chemistry [61].

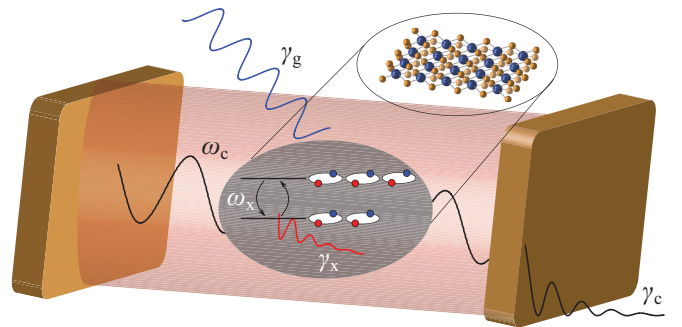


FIG. 1. Schematic of the explored strong-coupling cavities: a typical cavity formed by two mirrors, supporting a single optical mode with frequency  $\omega_c$  and damping rate  $\gamma_c$ . Gain is provided to it externally, at a rate  $\gamma_g$ . A QE system with a composite-bosonic character, formed by collective excitonic resonances in extended systems such as TMDs (as shown in the zoom-in sketch), with transition frequency  $\omega_x$  and damping rate  $\gamma_x$ , is placed between the mirrors and couples to the cavity mode with coupling constant  $g$ .

To describe the dynamics of the coupled system, we first assume for simplicity a perfect frequency alignment between the cavity and the exciton; this zero detuning is what most experiments try to achieve, so as to better evaluate the coupling properties [62–64]. Without loss of generality, we can then measure all energies with respect to this frequency, i.e., set  $\omega_c = \omega_x = 0$ . We focus on time-harmonic solutions of the form  $e^{-i\omega t}$ , and introduce frequencies and times normalised to the linewidth of the exciton system:  $\Omega \equiv 2\omega/\gamma_x$  and  $\tau \equiv \gamma_x t/2$ . Likewise, we introduce the normalised coupling  $G \equiv 2g/\gamma_x$ , and the normalised damping rate  $\Gamma \equiv (\gamma_g - \gamma_c)/\gamma_x$ . In what follows, we will explore the dynamics as  $\Gamma$  varies from  $-1$  (e.g., cavity in the absence of gain and with a linewidth matching that of the QE) to  $+1$  (i.e., where the gain not only compensates the cavity losses, but also exactly balances the broadening of the exciton), thus producing long-lived Rabi-like oscillations. The time-harmonic solutions are now governed by the dimensionless eigenvalue

problem

$$\begin{pmatrix} i\Gamma & G \\ G & -i \end{pmatrix} \begin{pmatrix} a(\tau) \\ b(\tau) \end{pmatrix}_{\pm} = \Omega_{\pm} \begin{pmatrix} a(\tau) \\ b(\tau) \end{pmatrix}_{\pm}, \quad (2)$$

whose diagonalisation yields the eigenfrequencies

$$\Omega_{\pm} = -\frac{i}{2}(1 - \Gamma) \pm \frac{1}{2}\sqrt{4G^2 - (1 + \Gamma)^2}. \quad (3)$$

In these dimensionless parameters, the Rabi-like frequency  $\Omega_R = \Omega_+ - \Omega_-$  becomes

$$\Omega_R = \sqrt{4G^2 - (1 + \Gamma)^2}, \quad (4)$$

which is a generalisation of the familiar result  $\Omega_R = 2G$  (for  $\Gamma = -1$  only). However, the introduction of gain also opens the possibility for an EP, the condition being  $\Gamma = \pm 2G - 1$  (which corresponds to  $\gamma_g = \pm 4g + \gamma_c - \gamma_x$ ). This condition dictates the transition between an oscillating and an overdamped (OD) system, shown by a blue dashed line in the coupling map shown in Fig. 2. When this is fulfilled, the square root vanishes, leading to vanishing splitting  $\Omega_R = 0$ . In fact, the fulfillment of the aforementioned condition, i.e.,  $2G = |\Gamma + 1|$ , corresponds to a manifold of exceptional points, where the  $\mathcal{PT}$  symmetry leads to coalescent eigenstates with entirely real eigenvalues  $\Omega_{\pm} = 0$ . Hereafter, in our analysis we focus on one of such EPs, namely that defined by  $G = \Gamma = 1$ , and henceforth denoted EP\*, which corresponds to a scenario where the gain exactly balances the combined losses associated with the linewidths of the cavity and emitter. As we shall see below, this point has intriguing consequences for the dynamics of the ensuing light-matter interaction. Finally, based on Eq. (3), one can define the amplification (AMP) region through  $\text{Im}\Omega_{\pm} > 0$ . One such AMP region, for which  $\Gamma < 1$  and  $(1 + \Gamma)^2 > 4G^2$ , is highlighted with light-red colour in the top-left corner of Fig. 2—it lies, nevertheless, still in the OD regime.

### III. VISIBILITY MEASURE

Before considering specific values of the normalised gain and exploring how they affect the QE-cavity coupling, it is useful to introduce a visibility measure for the Rabi oscillations in terms of the quality factor  $Q_R = \text{Re}[\Omega_- - \Omega_+] / \text{Im}[\Omega_- + \Omega_+]$ . Such quality factors have already been introduced in recent literature to deal with gainless strongly-coupled systems [22, 65], but here we generalise their applicability to the case of cavities with gain. From Eq. (3), we straightforwardly obtain (while also assuming  $2G \geq |1 + \Gamma|$ )

$$Q_R = \frac{\sqrt{4G^2 - (1 + \Gamma)^2}}{1 - \Gamma} = \frac{\sqrt{(4g)^2 - (\gamma_x + \gamma_g - \gamma_c)^2}}{\gamma_x - \gamma_g + \gamma_c}. \quad (5)$$

In the spirit of ring-down spectroscopy [75], this quality factor quantifies the number of “round trips”, i.e., the number of resolvable oscillations of light between the cavity and the emitter. In passing, we emphasise how the linewidths are naturally added up in accordance with Matthiessen’s rule for the addition of scattering rates [76]. Introduction of this measure for the visibility of Rabi-like oscillations allows us to rigorously discuss the weak-coupling (WC) versus strong-coupling (SC) regimes. Strong coupling occurs for  $Q_R > 1$ , corresponding to  $G > \sqrt{(1 + \Gamma^2)/2}$  (white region in Fig. 2), which is perfectly in line with the more common definition that the splitting should exceed the linewidth [1]. On the other hand, for  $Q_R < 1$  the dynamics will have all the characteristics associated with the WC regime (light-green area in the left part of Fig. 2); as  $Q_R$  approaches zero, the system enters either an overdamped regime (OD, blue triangular regions at the leftmost end of Fig. 2), or the regime with net amplification, depending on the relative gain. This is summarised in the parameter phase-space of Fig. 2, which provides a direct and intuitive guide for manipulating the coupling via application of gain. The black curves in the figure correspond to iso-contours of  $Q_R$  (values given with numbers in black font), while the dotted red curves are isofrequency contours, for the  $\Omega_R$  values given at the bottom of each curve in red font.

To evaluate the usefulness of  $Q_R$ , it is insightful to examine how state-of-the-art experiments from literature classify according to this measure. Such a comparison is done in Table I for a variety of QEs and cavities, most of which employ surface plasmons or localised plasmon resonances in nanoparticles as cavities, except for a one-dimensional photonic crystal in Ref. [68], and quantum optical systems in Refs. [72–74]. None of the experiments listed in the table have used gain, meaning that the listed  $\Gamma$  corresponds to the normalised damping rate of the cavity alone (i.e.,  $\Gamma = -\gamma_c/\gamma_x$ ). Using then this  $\Gamma$  together with  $\gamma_x$ , one can straightforwardly estimate if the usual strong-coupling criterion

$$\Omega_R > \frac{\gamma_x + \gamma_c}{2} \quad (6)$$

holds. This criterion is not normalised to any intrinsic property of the system, and it is therefore difficult to use it to compare different types of strong-coupling configurations, whereas  $Q_R$  is properly normalised and can then be applied to a wide variety of systems. Hence, the predictions of Eq. (6) do not strictly follow the computed  $Q_R$  appearing in the table.

Inspecting Table I, it appears that the highest  $Q_R (\geq 3)$  for nanophotonic systems are still achieved by architectures employing  $J$ -aggregates coupled to plasmonic systems [15, 16, 62]. This excellent performance is related to the high out-of-plane dipole-moments of the  $J$ -aggregated molecules, and the intense near fields provided by the plasmonic cavities. TMD-based systems, on the other hand, seem to be the most poorly perform-

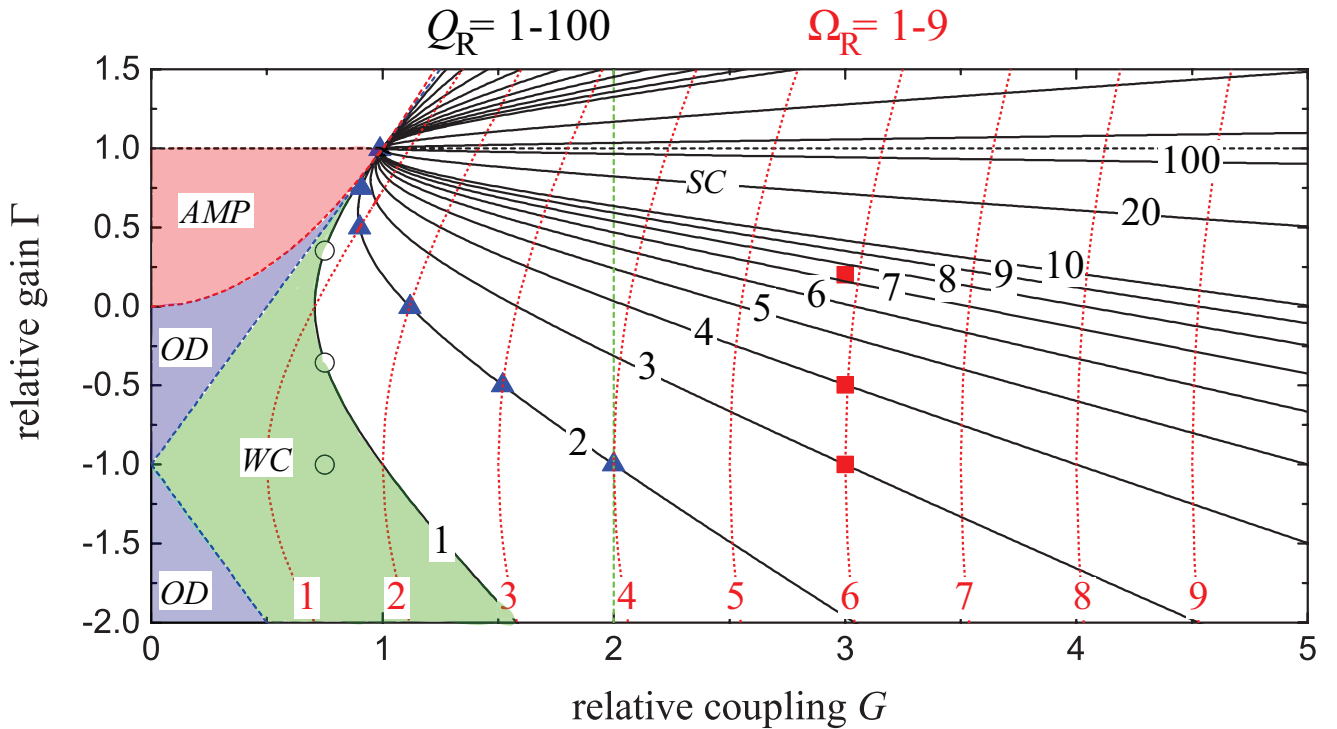


FIG. 2. Rabi-oscillation visibility quality factor ( $Q_R$ ) as a function of the relative gain ( $\Gamma$ ) and relative coupling ( $G$ ). Partial loss compensation occurs whenever  $\Gamma > -1$ , with  $\Gamma = 0$  corresponding to the case of a gain-balanced cavity ( $\gamma_g = \gamma_c$ ) and  $\Gamma = 1$  to the case of fully gain-compensated exciton-cavity system (i.e.,  $\gamma_g = \gamma_c + \gamma_x$ ). When  $2G = |\Gamma + 1|$  (blue dashed lines), the two solutions of Eq. (2) coalesce and give rise to EPs; the one at  $\Gamma = G = 1$  is particularly important and all  $Q_R$  isocontours cross it. The blue-shaded region (OD) is characterised by critical damping, while the red-shaded region (AMP) exhibits amplification. The weak-coupling regime (WC, green-shaded region) and the strong-coupling regime (SC, white region) are separated by the  $Q_R = 1$  curve. Black curves indicate isocontours corresponding to different  $Q_R$ , as indicated by the labels in black font; red dotted curves indicate isofrequency contours (constant  $\Omega_R$ ), with the (normalised) values of the frequencies labelled in red font. Open circles, blue triangles, and red squares correspond to specific  $G$  and  $\Gamma$  combinations discussed in the text.

ing at the moment. This has to do both with the fact that such activities have only recently emerged—leaving considerable room for improvement—but also with the fact that the effective dipole moment associated with excitons in these two-dimensional (2D) materials lie predominantly in plane, making the coupling with any out-of-plane cavity mode less efficient. In this respect, 2D halide perovskites, with their dipole moments oriented out of plane [77], might provide in the future an efficient alternative for 2D polaritonics [67, 78]. Similarly, high quality factors are also obtained for emitters based on 2D electron gases (2DEGs), in the case of either intersubband transitions [71] or cyclotron transitions [70]. Nevertheless, despite the recent advances in nanophotonics, the highest performance in terms of  $Q_R$  lies still in the quantum-optical domain, involving ultrahigh finesse (e.g. superconducting) cavities or Rydberg atoms. This is to be expected, since in those platforms the linewidths of both cavities and QEs can be very small, and all the experiments in Refs. [72–74] have been carried out at cryogenic temperatures. Of course, the requirement for such conditions, and the costs that accompany them, was one of the main motivation for shifting attention towards

room-temperature nanophotonics in the first place. One should thus always keep in mind the specific purpose that any new strong-coupling configuration would serve, and find the best balance between performance and cost. In passing, we should also mention that the values of relative  $\Gamma$  that we obtain by analysing the data reported in Refs. [72–74] are rather unconventional and unexpected (according to our previous definition, values below  $-1$  are expected for systems that are not externally pumped, while values between  $-1$  and  $0$  correspond to the presence of some kind of gain); these experiments typically involve single atoms and/or photons, and adoption of our  $Q_R$  measure should be done more judiciously.

#### IV. TIME EVOLUTION

In order to further substantiate the usefulness of the above visibility measure—also in the time domain—and to clearly display that the parameter space of Fig. 2 indeed quantifies the weak-versus-strong coupling regimes and the visibility of Rabi oscillations in the latter case, we next consider the time evolution of the cavity and emit-



Ref.	Cavity	Quantum Emitter	$g$ (meV)	$\gamma_x$ (meV)	$\gamma_c$ (meV)	$G$	$\Gamma$	$Q_R$
66	Localised plasmon resonance	TMD exciton	45	50	110	1.80	-2.2	1.1
64	Localised plasmon resonance	TMD exciton	64	28	170	4.57	-6.07	1.1
17	Localized plasmon resonance	$J$ -aggregate exciton	81	100	109	1.62	-1.09	1.6
67	Bragg mirror	Halide perovskite	48	90	25	1.06	-0.28	1.6
63	Plasmon-lattice resonance	$J$ -aggregate exciton	137.5	80	200	3.44	-2.50	1.9
68	Semiconductor microcavity	Organic semiconductor exciton	80	90	22	1.77	-0.24	2.8
19	Localised-plasmon resonance	Dye-molecule exciton	152.5	85	122	3.59	-1.44	2.9
15	Surface-plasmon resonance	$J$ -aggregate exciton	90	50	70	3.6	-1.4	3.0
62	Localised plasmon resonance	$J$ -aggregate exciton	200	100	150	4	-1.5	3.2
16	Surface-plasmon resonance	$J$ -aggregate exciton	125	$\sim 0.66$	$\sim 140$	380	-213	3.4
69	Plasmon-lattice resonance	$J$ -aggregate exciton	$\sim 350$	$\sim 20$	$\sim 200$	37.5	-10	4
70	THz metamaterial	2DEG cyclotron transition	$\sim 4.1$	$\sim 0.41$	$\sim 0.12$	20	-0.29	31
71	Semiconductor microcavity	2DEG intersubband transition	7	5	15	5.6	-3	45
72	Superconducting microcavity	Atomic beam	$2.9 \times 10^{-8}$	$2.1 \times 10^{-9}$	$1.7 \times 10^{-12}$	28	$-8.0 \times 10^{-4}$	56
73	Superconducting microcavity	Circular Rydberg atoms	$1.0 \times 10^{-7}$	$2.1 \times 10^{-11}$	$3.0 \times 10^{-9}$	$1.0 \times 10^4$	-145	137
74	Mirror cavity	Bose-Einstein condensate	$1.3 \times 10^{-3}$	$1.2 \times 10^{-5}$	$5.4 \times 10^{-6}$	213	-0.4	298

TABLE I. Table of strong-coupling experiments sorted by increasing  $Q_R$ . The similarity sign ( $\sim$ ) is used when the data listed in the table are not mentioned explicitly by the authors of the corresponding reference, but roughly estimated in this paper. In all of these experiments,  $\gamma_g = 0$ , and thus  $\Gamma = -\gamma_c/\gamma_x$ .

ter occupation numbers (herein non-normalised due to the semiclassical incorporation of gain). Starting with Eq. (1), the time evolution can be solved straightfor-

wardly (see Appendix A). For the initial conditions of an empty cavity and an excited emitter, i.e.,  $a(0) = 0$  and  $b(0) = 1$ , we find

$$|a(\tau)|^2 = \frac{4G^2}{\Omega_R^2} e^{-\frac{\Omega_R \tau}{Q_R}} \sin^2(\frac{1}{2}\Omega_R \tau) = \frac{2G^2}{\Omega_R^2} e^{-\frac{\Omega_R \tau}{Q_R}} [1 - \cos(\Omega_R \tau)] , \quad (7a)$$

$$|b(\tau)|^2 = e^{-\frac{\Omega_R \tau}{Q_R}} \left[ \cos(\Omega_R \tau) - \frac{(1 + \Gamma)}{\Omega_R} \sin(\Omega_R \tau) \right] + |a(\tau)|^2 . \quad (7b)$$

From these exact analytic expressions, it is unambiguously clear that the occupation numbers oscillate with a period governed solely by  $\Omega_R$ , while only a number of  $Q_R$  oscillations are visible, as a consequence of the overall exponential decaying factor  $e^{-\frac{\Omega_R \tau}{Q_R}}$ . Thus, our introduction of  $Q_R$  is more than a convenient parameterisation—it is the unique measure that emerges from a systematic dimensionless formulation of the problem. We emphasise that, while initially  $|a(0)|^2 + |b(0)|^2 = 1$ , there is no such conservation after a finite time. This is always anticipated in realistic systems due to the dispersive and lossy nature of the cavity and the QE; but in our case, because of the presence of gain, the sum of the two occupation numbers can, and indeed does, exceed unity. In what follows we will explore the dynamics of Eq. (7) for different limits of the parameter space depicted in Fig. 2, and discuss how the presence of gain can drastically affect the dynamics of the problem.

### 1. Weak-coupling dynamics

In the weak-coupling regime, with  $Q_R \ll 1$ , the general solution of Eq. (7) can be significantly simplified. This is the Weisskopf-Wigner regime [79], where the cavity exhibits an initial quadratic rise,

$$|a(\tau)|^2 \approx (G\tau)^2 e^{-\frac{\Omega_R \tau}{Q_R}} , \quad (8a)$$

where  $G$  naturally determines the rate of growth, while the accompanied initial dynamics of the QE is characterised by an exponential decay,

$$|b(\tau)|^2 \approx e^{-\frac{\Omega_R \tau}{Q_R}} = e^{-(1-\Gamma)\tau} . \quad (8b)$$

In Figs. 3(a)-(c) we show this dynamics for three values of  $\Gamma$  along the  $G = 0.75$  line in Fig. 2 (open circles). In panel (a), gain is completely absent ( $\Gamma = -1$ ), and the system is entirely characterised by its intrinsic loss,

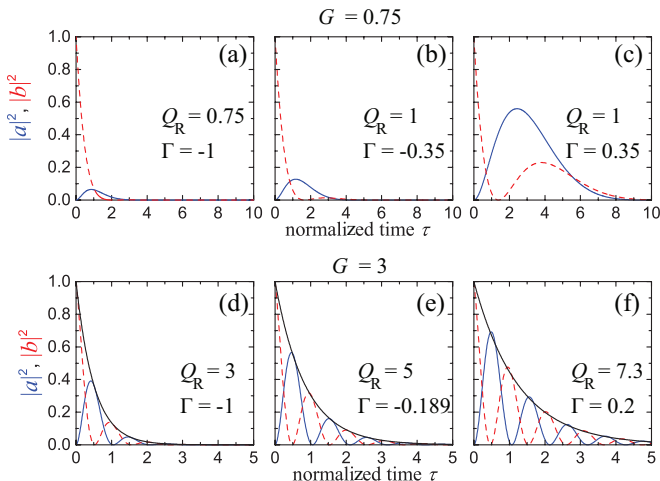


FIG. 3. Upper panel: dynamics of the occupation numbers  $|b(\tau)|^2$  (red dashed curve) and  $|a(\tau)|^2$  (blue solid curve), with initial conditions  $|b(0)|^2 = 1$  and  $|a(0)|^2 = 0$ , for three cases with  $G = 0.75$  (weak-coupling regime) and  $\Gamma = -1.0$  (a),  $\Gamma = -\sqrt{2}/4$  (b), and  $\Gamma = \sqrt{2}/4$  (c) (see open circles in Fig. 2). Lower panel: similar dynamics for the strong-coupling regime with  $G = 3$  and  $\Gamma = -1$  (d),  $\Gamma = -0.189$  (e), and  $\Gamma = 0.2$  (f) (see red squares in Fig. 2). Black curves in the last three panels show the exponential decay envelope of Eqs. (9).

leading to the anticipated exponential decay. Panel (b) corresponds to  $\Gamma = -\sqrt{2}/4 \simeq -0.35$  which, according to Eq. (5) translates into the first of the two points with  $Q_R = 1$ , the one still dominated by loss (i.e., with  $\Gamma < 0$ ). The emergence of a first oscillation in  $|b(\tau)|^2$  is indeed (hardly) discernible in the red dashed curve. Finally, panel (c) corresponds to  $\Gamma = \sqrt{2}/4 \simeq 0.35$ , i.e. the second condition for which  $Q_R = 1$  in Fig. 2; the external gain has now started driving the system, so that a full oscillation in  $|b(\tau)|^2$  can be observed before its eventual decay. According to Fig. 2, it is feasible to drive the system into the strong-coupling regime, just between these two points (before the  $Q_R = 1$  curve backbends again for higher gain). On the other hand, keeping  $G$  constant, say at 0.75, and moving vertically in Fig. 2, provides a recipe for tailoring the Purcell factor in the weak-coupling regime. The Purcell factor expresses the acceleration of the spontaneous emission rate in a cavity; the rate itself, is essentially proportional to the square of the coupling strength, and inversely proportional to the damping of the cavity [80]. Consequently, for a fixed  $G$ , Fig. 2 suggests that spontaneous emission rate increases, leading to a larger Purcell factor. Finally, it is also important to observe that the period of the oscillations has increased (in accordance with the shape of the isofrequency contours in this region), and the two populations are more in phase; this will become relevant again in the subsequent analysis.

## 2. Strong-coupling dynamics

Deep into the strong-coupling regime, where  $G \gg 1$ , Eqs. (7) simplify to

$$|a(\tau)|^2 \simeq e^{-\frac{\Omega_R \tau}{Q_R}} \sin^2\left(\frac{1}{2}\Omega_R \tau\right), \quad (9a)$$

$$|b(\tau)|^2 \simeq e^{-\frac{\Omega_R \tau}{Q_R}} \cos^2\left(\frac{1}{2}\Omega_R \tau\right). \quad (9b)$$

Here, we clearly see how the two occupation numbers evolve fully out of phase, i.e., energy bounces back and forth between the excitonic component and the cavity, while of course still being exponentially damped over time. In turn, these expressions imply that  $|a(\tau)|^2 + |b(\tau)|^2 \simeq e^{-\frac{\Omega_R \tau}{Q_R}}$ . This is the common strong-coupling dynamics [79]. Here, it is immediately evident that  $Q_R$  quantifies the number of oscillations before reaching full relaxation: what the addition of gain achieves is to increase the number of oscillations that are visible before complete decay. Corresponding results are shown in the lower half of Fig. 3, panels (d-f), for  $G = 3$  (red squares in Fig. 2). When the system is not compensated [ $\Gamma = -1$ , panel (d)], three oscillations are observable in the dynamics (the third only just). By increasing the amount of gain provided to the system, one can increase the longevity of the Rabi oscillations, and move vertically in the map of Fig. 2 (red squares), leading to more oscillations (still dominated by the same Rabi frequency, unlike in the previous case, as one can anticipate by observing the corresponding isofrequency contour which is nearly vertical) to be observed. The anticipated exponential decay is demonstrated in all three cases by the black curves.

## 3. Coalescing dynamics

A less explored special case, that only becomes relevant in the kind of cavities with gain that we study here, concerns the dynamics in the vicinity of an EP associated with  $\mathcal{PT}$  symmetry. Looking at Eqs. (7), we notice that, while  $|a(\tau)|^2 \propto \Omega_R^{-2}$ , the  $|b(\tau)|^2$  part contains terms scaling as  $\Omega_R^0$ ,  $\Omega_R^{-1}$ , and  $\Omega_R^{-2}$ . Approaching EP\* (i.e., the EP for which  $G = \Gamma = 1$ ), where  $\Omega_R \rightarrow 0$ , the  $\Omega_R^{-2}$  contribution dominates, and consequently  $|b(\tau)|^2 \rightarrow |a(\tau)|^2$ . This implies an intriguing in-phase time evolution of the occupation numbers, which is a remarkable consequence of  $\mathcal{PT}$  symmetry and the coalescing eigenstates at EPs.

To see how the dynamics changes as the EP\* is approached, we follow in Fig. 4 the  $Q_R = 2$  curve for increasing  $\Gamma$  (see blue triangles in Fig. 2). In the top three panels (a-c), the composite cavity is still lossy overall. In all cases, two oscillations are observed (the second one barely) as expected, but their period increases as the provided gain increases, in accordance with the behaviour of the weakly-coupled system of Fig. 3. This behaviour could be immediately anticipated based on the isofrequency contours of Fig. 2: following the  $Q_R = 2$  line

means crossing several of the dotted red contours, with the frequency decreasing as gain increases. In the lower panels (d-f) the system is practically externally driven by the gain. As the gain increases and the EP\* point is approached, the Rabi oscillations are further decelerated, both populations increase beyond the initial condition of unity, and their phase difference becomes ever smaller. Near EP\* (which cannot be reached exactly, so we can only approach it adiabatically), both populations oscillate practically in phase and coincide in their maximum values; the system is driven externally, and has approached the net amplification regime.

## V. RABI-OSCILLATION RETRIEVAL

The gain-induced changes in the dynamics discussed above suggest that one might be able to use gain to characterise the time evolution of the system even if its initial Rabi oscillations are too fast to be experimentally traceable [e.g., as in typical plasmon-exciton coupling systems where  $\Omega_R$  can be substantial (even though the corresponding  $Q_R$  are often modest due to the sizable  $\gamma_c$ )]. To this end, we plot in Fig. 5 the period of the oscillations as a function of the externally provided gain, for couplings ranging from  $G = 1 - 2.5$ . As the relative gain increases, one moves vertically along Fig. 2, meaning that  $Q_R$  is expected to increase rapidly, especially for relatively small  $G$ , for which the isofrequency contours are more curved. At the same time, following the previous discussion, the period of the oscillations is also expected to increase, since it is just  $T = 2\pi/\Omega_R$ , with  $\Omega_R$  given by Eq. (4). This is indeed shown in Fig. 5(a), for four cases of relatively small (yet larger than unity)  $G$ . One imme-

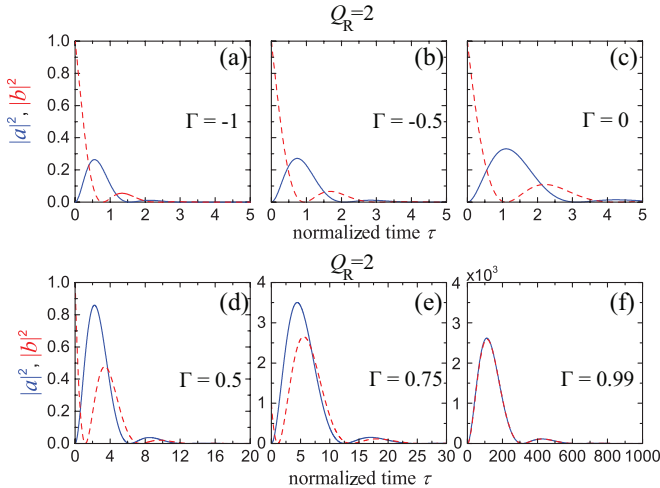


FIG. 4. Dynamics of the occupation numbers  $|b(\tau)|^2$  (red dashed curve) and  $|a(\tau)|^2$  (blue solid curve), with initial conditions  $|b(0)|^2 = 1$  and  $|a(0)|^2 = 0$ , for six cases on the  $Q_R = 2$  contour with  $\Gamma = -1$  (a),  $\Gamma = -0.5$  (b),  $\Gamma = 0$  (c),  $\Gamma = 0.5$  (d),  $\Gamma = 0.75$  (e), and  $\Gamma = 0.99$  (f), see blue triangles in Fig. 2.

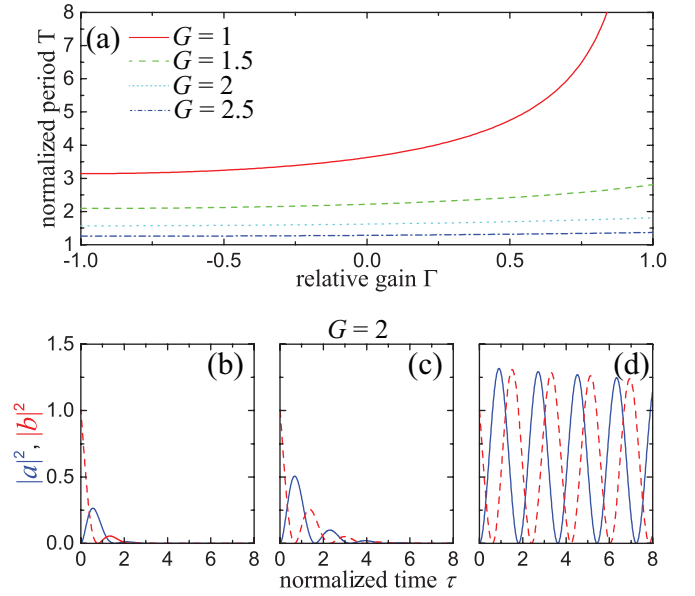


FIG. 5. (a) Normalised period of the Rabi oscillations for a QE-cavity system with  $G$  equal to 1 (solid red line) to 1.5 (dashed green line), 2 (light-blue dotted line), and 2.5 (dashed-dotted blue line) as a function of the externally provided normalised gain  $\Gamma$ . The period clearly follows an inverse square-root law, in agreement with Eq. (4). (b)-(d) Time dynamics of the occupation numbers  $|b(\tau)|^2$  (red dashed curves) and  $|a(\tau)|^2$  (blue solid curves), with initial conditions  $|b(0)|^2 = 1$  and  $|a(0)|^2 = 0$ , for  $G = 2$  and  $\Gamma = -1$  (b),  $\Gamma = 0$  (c), and  $\Gamma = 0.99$  (d).

diately observes that the weaker the coupling, the more it can be affected by the exertion of gain, again in agreement with the isofrequency contours of Fig. 2. Three typical examples of the dynamics are shown in panels (b-d), for  $G = 2$  (along the vertical dashed green line in the middle of Fig. 2), where the relative gain increases from  $\Gamma = -1.0$  (no gain) to  $\Gamma = 0$  (fully compensated cavity) and  $\Gamma = 0.99$  (gain-dominated cavity). As discussed above, not only does the number of observable Rabi oscillations increase, but they are also decelerated (i.e., their period increases), while eventually the populations exceed unity as expected.

What one can immediately observe in the dynamics of Fig. 5(a) is that the period of the oscillations follows an inverse-square dependence on  $\Gamma$ , as expected from Eq. (4), and as one can retrieve by calculating specific examples of dynamics. This suggests a way to deduce the period of Rabi oscillations in ultrafast QE-cavity systems, where the oscillations, with periods of a few fs, cannot be resolved with current instruments. But in a loss-compensated cavity, where the gain is externally controlled, one can increase the period of the oscillations to the point where the instrument resolution allows clear observation of the dynamics, and then extrapolate to the expected value in the absence of gain. Gain-dominated cavities provide thus the means to not only manipulate the dynamics of the QE-cavity system, but potentially

also characterise it through gradual modification of the provided gain.

## VI. CONCLUSION

We have analysed the dynamics of QEs coupled to optical cavities that can be controlled via externally-provided gain. Based on a general Rabi-visibility criterion that quantifies the number of oscillations one should expect to observe in an experiment, we established three different coupling regimes, namely weak, strong, and coalescing. We showed that the provided gain affects differently these three regimes. When the coupling strength ( $G$ ) is large, the dynamics (and particularly the period of Rabi oscillations) is not considerably affected by gain, and only the populations of the ground and excited states change, being allowed to exceed unity. On the other hand, for weak and intermediate coupling strengths, externally pumping the system eventually governs the dynamics, and the period of the Rabi oscillations increases, suggesting that one could use gain to resolve ultrafast dynamics by controllably and reversibly accelerating and decelerating the oscillations. Finally, in the coalescing regime, near the EP of the resulting  $\mathcal{PT}$ -symmetric cavity, all system dynamics is completely governed by gain, both populations oscillate nearly in phase, and they are allowed to dramatically exceed unity. Such dynamics opens up new possibilities for the design of dynamically controlled cavities for strong-coupling realisations.

## ACKNOWLEDGMENTS

We thank P. Edderkop for assistance with preparation of the graphs and the web design. C. W. and F. T. acknowledge funding from MULTIPLY fellowships under the Marie Skłodowska-Curie COFUND Action (grant agreement No. 713694). M. H. E. acknowledges funding from Independent Research Fund Denmark (Grant No. 0165-00051B). N. A. M. is a VILLUM Investigator supported by VILLUM Fonden (grant No. 16498). The Center for Polariton-driven Light-Matter Interactions (POLIMA) is sponsored by the Danish National Research Foundation (Project No. DNRF165).

### Appendix A: Details on time evolution

The dynamics of the coupled QE-cavity system are governed by the linear system typified by Eq. (1). Under the conditions considered in the main text (i.e.,  $\omega_c = \omega_x = 0$ ) and using the dimensionless quantities introduced in the same, we have

$$\frac{\partial}{\partial \tau} \begin{pmatrix} a(\tau) \\ b(\tau) \end{pmatrix} = \begin{pmatrix} \Gamma & -iG \\ -iG & -1 \end{pmatrix} \begin{pmatrix} a(\tau) \\ b(\tau) \end{pmatrix}, \quad (\text{A1a})$$

which we write compactly as

$$\dot{\mathbf{x}}(\tau) = \mathbf{A} \mathbf{x}(\tau). \quad (\text{A1b})$$

The determination of the time evolution of the state vector  $\mathbf{x}(\tau)$  can be straightforwardly calculated once in possession of the eigenvalues ( $\lambda_{\pm}$ ) and the eigenvectors ( $\mathbf{v}_{\pm}$ ) of  $\mathbf{A}$ , which read

$$\lambda_{\pm} = \frac{\Gamma - 1}{2} \pm \frac{1}{2} \sqrt{(\Gamma + 1)^2 - 4G^2} = i\Omega_{\pm} \quad (\text{A2a})$$

and

$$\mathbf{v}_{\pm} = \mathcal{N}_{\pm} \begin{pmatrix} i\frac{\Gamma + 1 \pm \sqrt{(\Gamma + 1)^2 - 4G^2}}{2G}, 1 \end{pmatrix}^T, \quad (\text{A2b})$$

respectively; here,  $\mathcal{N}_{\pm}$  are normalization constants.

Equipped with the eigenvalues and eigenvectors of  $\mathbf{A}$  [cf. Eqs. (A1)–(A2)], the time evolution of the system follows from

$$\mathbf{x}(\tau) \equiv \begin{pmatrix} a(\tau) \\ b(\tau) \end{pmatrix} = C_1 e^{\lambda_- \tau} \mathbf{v}_- + C_2 e^{\lambda_+ \tau} \mathbf{v}_+, \quad (\text{A3})$$

that is,

$$a(\tau) = C_1 e^{\lambda_- \tau} \mathcal{N}_- \left( i\frac{\Gamma + 1 - \eta}{2G} \right) + C_2 e^{\lambda_+ \tau} \mathcal{N}_+ \left( i\frac{\Gamma + 1 + \eta}{2G} \right), \quad (\text{A4a})$$

$$b(\tau) = C_1 e^{\lambda_- \tau} \mathcal{N}_- + C_2 e^{\lambda_+ \tau} \mathcal{N}_+, \quad (\text{A4b})$$

where we have introduced  $\eta = \sqrt{(\Gamma + 1)^2 - 4G^2}$  for shorthand notation. The constants  $C_{1,2}$  are determined by the initial conditions; hereafter, we assume that the emitter-cavity system is initially in the state  $\mathbf{x}_0 \equiv \mathbf{x}(\tau_0 = 0) = (a(0), b(0))^T = (0, 1)^T$ , corresponding to an empty cavity and all the population is in the emitter. The choice of these initial conditions implies that

$$C_1 = \frac{\Gamma + 1 + \eta}{2\eta \mathcal{N}_-}, \quad C_2 = -\frac{\Gamma + 1 - \eta}{2\eta \mathcal{N}_+}. \quad (\text{A5})$$

Then, substituting Eqs. (A5) into Eqs. (A4), yields

$$a(\tau) = \frac{iG}{\eta} [e^{\lambda_- \tau} - e^{\lambda_+ \tau}], \quad (\text{A6a})$$

$$b(\tau) = \frac{\Gamma + 1}{2\eta} [e^{\lambda_- \tau} - e^{\lambda_+ \tau}] + \frac{1}{2} [e^{\lambda_- \tau} + e^{\lambda_+ \tau}]. \quad (\text{A6b})$$

Moreover, noting that  $\lambda_{\pm} = i\Omega_{\pm}$  and  $\eta = i\Omega_R$  as well as  $1 - \Gamma = \Omega_R/Q_R$ , Eqs. (A6) can be written as

$$a(\tau) = -\frac{2iG}{\Omega_R} \sin\left(\frac{\Omega_R}{2}\tau\right) e^{-\frac{\Omega_R \tau}{2Q_R}}, \quad (\text{A7a})$$

$$b(\tau) = \left\{ -\frac{\Gamma + 1}{\Omega_R} \sin\left(\frac{\Omega_R}{2}\tau\right) + \cos\left(\frac{\Omega_R}{2}\tau\right) \right\} e^{-\frac{\Omega_R \tau}{2Q_R}}, \quad (\text{A7b})$$

which are the sought-after amplitudes governing the time evolution of the coupled QE-cavity system [cf. Eqs. (7)].



\* Present address: ICFO — Institut de Ciències Fotòniques, The Barcelona Institute of Science and Technology, 08860 Castelldefels (Barcelona), Spain

- [1] P. Törmä and W. L. Barnes, *Rep. Prog. Phys.* **78**, 013901 (2015).
- [2] P. Vasa and C. Lienau, *ACS Photonics* **5**, 2 (2018).
- [3] C. Tserkezis, A. I. Fernández-Domínguez, P. A. D. Gonçalves, F. Todisco, J. D. Cox, K. Busch, N. Stenger, S. I. Bozhevolnyi, N. A. Mortensen, and C. Wolff, *Rep. Prog. Phys.* **83**, 082401 (2020).
- [4] J. Sun, Y. Li, H. Hu, W. Chen, D. Zheng, S. Zhang, and H. Xu, *Nanoscale* **13**, 4408 (2021).
- [5] X. Xiong, N. Kongsuwan, Y. Lai, C. E. Png, L. Wu, and O. Hess, *Appl. Phys. Lett.* **118**, 130501 (2021).
- [6] P. Dombi, Z. Pápa, J. Vogelsang, S. V. Yalunin, M. Sivilis, G. Herink, S. Schäfer, P. Groß, C. Ropers, and C. Lienau, *Rev. Mod. Phys.* **92**, 025003 (2020).
- [7] A. I. Fernández-Domínguez, S. I. Bozhevolnyi, and N. A. Mortensen, *ACS Photonics* **5**, 3447 (2018).
- [8] E. M. Purcell, *Phys. Rev.* **68**, 681 (1946).
- [9] H. Walther, B. T. H. Varcoe, B.-G. Englert, and T. Becker, *Rep. Prog. Phys.* **69**, 1325 (2006).
- [10] A. F. Kockum, A. Miranowicz, S. De Liberato, S. Savasta, and F. Nori, *Nat. Rev. Phys.* **1**, 19 (2019).
- [11] S. Haroche and D. Kleppner, *Phys. Today* **42**(1), 24 (1989).
- [12] C. Weisbuch, M. Nishioka, A. Ishikawa, and Y. Arakawa, *Phys. Rev. Lett.* **69**, 3314 (2013).
- [13] T. Yoshie, A. Scherer, J. Hendrickson, G. Khitrova, H. M. Gibbs, G. Rupper, C. Ell, O. B. Shchekin, and D. G. Deppe, *Nature* **432**, 200 (2004).
- [14] P. A. D. Gonçalves, N. Stenger, J. D. Cox, N. A. Mortensen, and S. Xiao, *Adv. Opt. Mater.* **8**, 1901473 (2020).
- [15] J. Bellessa, C. Bonnand, J. C. Plenet, and J. Mugnier, *Phys. Rev. Lett.* **93**, 036404 (2004).
- [16] J. Dintinger, S. Klein, F. Bustos, W. L. Barnes, and T. W. Ebbesen, *Phys. Rev. B* **71**, 035424 (2005).
- [17] G. Zengin, M. Wersäll, S. Nilsson, T. J. Antosiewicz, M. Käll, and T. Shegai, *Phys. Rev. Lett.* **114**, 157401 (2015).
- [18] Y. Sugawara, T. A. Kelf, J. J. Baumberg, M. E. Abdelsalam, and P. N. Bartlett, *Phys. Rev. Lett.* **97**, 266808 (2006).
- [19] R. Chikkaraddy, B. de Nijs, F. Benz, S. J. Barrow, O. A. Scherman, E. Rosta, A. Demetriadou, P. Fox, O. Hess, and J. J. Baumberg, *Nature* **535**, 127 (2016).
- [20] K. Santhosh, O. Bitton, L. Chuntunov, and G. Haran, *Nat. Commun.* **7**, 11823 (2016).
- [21] C. Tserkezis, P. A. D. Gonçalves, C. Wolff, F. Todisco, K. Busch, and N. A. Mortensen, *Phys. Rev. B* **98**, 155439 (2018).
- [22] F. Todisco, R. Malureanu, C. Wolff, P. A. D. Gonçalves, A. S. Roberts, N. A. Mortensen, and C. Tserkezis, *Nanophotonics* **9**, 803 (2020).
- [23] G. W. Castellanos, S. Murai, T. V. Raziman, S. Wang, M. Ramezani, A. G. Curto, and J. Gómez Rivas, *ACS Photonics* **7**, 1226 (2020).
- [24] S. Shen, Y. Wu, Y. Li, P. Xie, Q. Ding, X. Kuang, W. Wang, and W. Wang, *Phys. Rev. B* **105**, 155403 (2022).
- [25] B. Gurlek, V. Sandoghdar, and D. Martín-Cano, *ACS Photonics* **5**, 456 (2018).
- [26] P. E. Stamatopoulou, V. Yannopapas, N. A. Mortensen, and C. Tserkezis, *Phys. Rev. B* **102**, 195415 (2020).
- [27] P. E. Stamatopoulou, S. Droulias, G. P. Acuna, N. A. Mortensen, and C. Tserkezis, *Nanoscale* **14**, 17581 (2022).
- [28] F. J. García-Vidal, C. Ciuti, and T. W. Ebbesen, *Science* **373**, eabd0336 (2021).
- [29] C. M. Bender, *Rep. Prog. Phys.* **70**, 947 (2007).
- [30] R. El-Ganainy, K. G. Makris, M. Khajavikhan, Z. H. Musslimani, S. Rotter, and D. N. Christodoulides, *Nat. Phys.* **14**, 11 (2018).
- [31] C. M. Bender and S. Boettcher, *Phys. Rev. Lett.* **80**, 5243 (1998).
- [32] K. G. Makris, R. El-Ganainy, D. N. Christodoulides, and Z. H. Musslimani, *Phys. Rev. Lett.* **100**, 103904 (2008).
- [33] A. Guo, G. J. Salamo, D. Duchesne, R. Morandotti, M. Volatier-Ravat, V. Aimez, G. A. Siviloglou, and D. N. Christodoulides, *Phys. Rev. Lett.* **103**, 093902 (2009).
- [34] H. Ramezani, T. Kottos, R. El-Ganainy, and D. N. Christodoulides, *Phys. Rev. A* **82**, 043803 (2010).
- [35] L. Feng, Y.-L. Xu, W. S. Fegadolli, M.-H. Lu, J. E. B. Oliveira, V. R. Almeida, Y.-F. Chen, and A. Scherer, *Nat. Mater.* **12**, 108 (2013).
- [36] B. Peng, Ş. K. Özdemir, F. Lei, F. Monifi, M. Gianfreda, G. L. Long, S. Fan, F. Nori, C. M. Bender, and L. Yang, *Nat. Phys.* **10**, 394 (2014).
- [37] Y. Huang, G. Veronis, and C. Min, *Opt. Express* **23**, 29882 (2015).
- [38] Z. Lin, H. Ramezani, T. Eichelkraut, T. Kottos, H. Cao, and D. N. Christodoulides, *Phys. Rev. Lett.* **106**, 213902 (2011).
- [39] D. L. Sounas, R. Fleury, and A. Alù, *Phys. Rev. Appl.* **4**, 014005 (2015).
- [40] L. Feng, Z. J. Wong, R.-M. Ma, Y. Wang, and X. Zhang, *Science* **346**, 972 (2014).
- [41] H. Hodaie, M.-A. Miri, M. Heinrich, D. N. Christodoulides, and M. Khajavikhan, *Science* **346**, 975 (2014).
- [42] Z. Gao, S. T. M. Fryslie, B. J. Thompson, P. S. Carney, and K. D. Choquette, *Optica* **4**, 323 (2017).
- [43] M. P. Hokmabadi, A. Schumer, D. N. Christodoulides, and M. Khajavikhan, *Nature* **576**, 70 (2019).
- [44] S. Sanders and A. Manjavacas, *Nanophotonics* **9**, 473 (2020).
- [45] J. Wiersig, *Phys. Rev. Lett.* **112**, 203901 (2014).
- [46] H. Hodaie, A. U. Hassan, S. Wittek, H. Garcia-Gracia, R. El-Ganainy, D. N. Christodoulides, and M. Khajavikhan, *Nature* **548**, 187 (2017).
- [47] W. Chen, Ş. K. Özdemir, G. Zhao, J. Wiersig, and L. Yang, *Nature* **548**, 192 (2017).
- [48] N. A. Mortensen, P. A. D. Gonçalves, M. Khajavikhan, D. N. Christodoulides, C. Tserkezis, and C. Wolff, *Optica* **5**, 1342 (2018).
- [49] J. Wiersig, *Photon. Res.* **8**, 1457 (2020).
- [50] S. N. Ghosh and Y. D. Chong, *Sci. Rep.* **6**, 19837 (2016).
- [51] A. V. Sadovnikov, A. A. Zyablovsky, A. v. Dorofeenko, and S. A. Nikitov, *Phys. Rev. Appl.* **18**, 024073 (2022).
- [52] V. M. Agranovich, M. Litinskaia, and D. G. Lidzey, *Phys. Rev. B* **67**, 085311 (2003).

- [53] S. Franke, J. Ren, and S. Hughes, *Phys. Rev. A* **105**, 023702 (2022).
- [54] S. Fan, W. Suh, and J. D. Joannopoulos, *J. Opt. Soc. Am. A* **20**, 569 (2003).
- [55] Excitons, being quasiparticles made of two elementary fermions, are often well-described as *composite* bosons [81] and thus exhibiting bosonic character (bosonic commutation relations [82], Bose–Einstein condensation [83], etc.) in the low-density limit. In some circumstances, however, they can behave more like fermions or even exhibit mixed bosonic and fermionic effects [84, 85].
- [56] Y. Li, X. Ma, Z. Hatzopoulos, P. G. Savvidis, S. Schumacher, and T. Gao, *ACS Photonics* **9**, 2079 (2022).
- [57] J. J. Geuchies, B. Brynjarsson, G. Grimaldi, S. Gudjonsdottir, W. van der Stam, W. H. Evers, and A. J. Houtepen, *ACS Nano* **15**, 377 (2021).
- [58] S. Morozov, C. Wolff, and N. A. Mortensen, *Adv. Opt. Mater.* **9**, 2101305 (2021).
- [59] R. C. Keitel, M. Aellen, B. le Feber, A. A. Rossinelli, S. A. Meyer, J. Cui, and D. J. Norris, *Nano Lett.* **21**, 8952 (2021).
- [60] R. R. Cooney, S. L. Sewall, D. M. Sagar, and P. Kambhampati, *Phys. Rev. Lett.* **102**, 127404 (2009).
- [61] I. B. Martini, I. M. Craig, W. C. Molenkamp, H. Miyata, S. H. Tolbert, and B. J. Schwartz, *Nat. Nanotechnol.* **2**, 647 (2007).
- [62] M. Wersäll, J. Cuadra, T. J. Antosiewicz, S. Balci, and T. Shegai, *Nano Lett.* **17**, 551 (2017).
- [63] F. Todisco, M. De Giorgi, M. Esposito, L. De Marco, A. Zizzari, M. Bianco, L. Dominici, D. Ballarini, V. Arima, G. Gigli, and D. Sanvitto, *ACS Photonics* **5**, 143 (2018).
- [64] M. Geisler, X. Cui, J. Wang, T. Rindzevicius, L. Gammegaard, B. S. Jessen, P. A. D. Gonçalves, F. Todisco, P. Bøggild, A. Boisen, M. Wubs, N. A. Mortensen, S. Xiao, and N. Stenger, *ACS Photonics* **6**, 994 (2019).
- [65] Z.-J. Yang, T. J. Antosiewicz, and T. Shegai, *Opt. Express* **24**, 20373 (2016).
- [66] M. Stührenberg, B. Munkhbat, D. G. Baranov, J. Cuadra, A. B. Yankovich, T. J. Antosiewicz, E. Olsson, and T. Shegai, *Nano Lett.* **18**, 5938 (2019).
- [67] P. Bouteyre, H. S. Nguyen, J.-S. Lauret, G. Trippé=Allard, G. Delport, F. Lédée, H. Diab, A. Belarouci, C. Seassal, D. Garrot, F. Bretenaker, and E. Deleporte, *ACS Photonics* **6**, 1804 (2019).
- [68] D. G. Lidzey, D. D. C. Bradley, M. S. Skolnick, T. Virgili, S. Walker, and D. M. Whittaker, *Nature* **395**, 53 (1998).
- [69] P. Vasa, W. Wang, R. Pomraenke, M. Lammers, M. Maiuri, C. Manzoni, G. Cerullo, and C. Lienau, *Nat. Photon.* **7**, 128 (2013).
- [70] G. Scalari, C. Maissen, D. Turčínková, D. Hagenmüller, S. De Liberato, C. Ciuti, C. Reichl, D. Schuh, W. Wegscheider, M. Beck, and J. Faist, *Science* **335**, 1323 (2012).
- [71] D. Dini, R. Köhler, A. Tredicucci, G. Biasiol, and L. Sorba, *Phys. Rev. Lett.* **90**, 116401 (2003).
- [72] G. Rempe, F. Schmidt-Kaler, and H. Walther, *Phys. Rev. Lett.* **64**, 2783 (1990).
- [73] M. Brune, F. Schmidt-Kaler, A. Maali, J. Dreyer, E. Hagley, J. M. Raimond, and S. Haroche, *Phys. Rev. Lett.* **76**, 1800 (1996).
- [74] F. Brennecke, T. Donner, S. Ritter, T. Bourdel, M. Köhl, and T. Esslinger, *Nature* **450**, 268 (2007).
- [75] A. Maity, S. Maithani, and M. Pradhan, *Anal. Chem.* **93**, 388 (2021).
- [76] N. W. Ashcroft and N. D. Mermin, *Solid State Physics* (Harcourt, Orlando, 1976).
- [77] L. Mao, C. C. Stoumpos, and M. G. Kanatzidis, *J. Am. Chem. Soc.* **141**, 1171 (2019).
- [78] R. Su, A. Fieramosca, Q. Zhang, H. S. Nguyen, E. Deleporte, Z. Chen, D. Sanvitto, T. C. H. Liew, and Q. Xiong, *Nat. Mater.* **10**, 1315 (2021).
- [79] M. O. Scully and M. S. Zubairy, *Quantum Optics* (Cambridge University Press, Cambridge, 1997).
- [80] G. S. Agarwal, *Quantum Optics* (Cambridge University Press, Cambridge, 2013).
- [81] M. Combescot and S.-Y. Shiau, *Excitons and Cooper Pairs: Two Composite Bosons in Many-Body Physics* (Oxford University Press, 2015).
- [82] F. Katsch, M. Selig, A. Carmele, and A. Knorr, *Phys. Stat. Sol. (b)* **255**, 1800185 (2018).
- [83] V. M. Pereira, *Nat. Phys.* **18**, 6 (2021).
- [84] M. Combescot, M. Betbeder-Matibet, and F. Dubin, *Phys. Rep.* **463**, 215 (2008).
- [85] M. Katzer, M. Selig, L. Sigl, M. Troue, J. Figueiredo, J. Kiemle, F. Sigger, U. Wurstbauer, A. W. Holleitner, and A. Knorr, *arXiv* , 2303.11787 (2023).

